Identifying the neutrino mass hierarchy with supernova neutrinos

R. Tomàs
AHEP Group - Institut de Física Corpuscular (CSIC - Universitat de València)
Apartat de Correus 22085, E-46071 València, SPAIN

We review how a high-statistics observation of the neutrino signal from a future galactic core-collapse supernova (SN) may be used to discriminate between different neutrino mixing scenarios. Most SN neutrinos are emitted in the accretion and cooling phase, during which the flavor-dependent differences of the emitted neutrino spectra are small and rather uncertain. Therefore the discrimination between neutrino mixing scenarios using these neutrinos should rely on observables independent of the SN neutrino spectra. We discuss two complementary methods that allow for the positive identification of the mass hierarchy without knowledge of the emitted neutrino fluxes, provided that the 13-mixing angle is large, $\sin^2\theta_{13} \gg 10^{-5}$. These two approaches are the observation of modulations in the neutrino spectra by Earth matter effects or by the passage of shock waves through the SN envelope. If the value of the 13-mixing angle is unknown, using additionally the information encoded in the prompt neutronization ν_e burst—a robust feature found in all modern SN simulations—can be sufficient to fix both the neutrino hierarchy and to decide whether θ_{13} is "small" or "large."

IFIC/07-01

I. INTRODUCTION

Despite the enormous progress of neutrino physics in the last decade, many open questions remain to be solved. Among them are two, the mass hierarchy—normal versus inverted mass spectrum—and the value of the 13-mixing angle θ_{13}, where the observation of neutrinos from a core-collapse supernova (SN) could provide important clues [1, 2, 3]. Schematically, the neutrino emission by a SN can be divided into four stages: Infall phase, neutronization burst, accretion, and Kelvin-Helmholtz cooling phase. During the infall phase and neutronization burst only ν_e's are emitted, while the bulk of neutrino emission is released in all flavors in the two latest phases. Whereas the neutrino emission characteristics of the two initial stages are basically independent of the features of the progenitor, such as its mass or equation of state (EoS) of the core, the details of the neutrino fluxes during the accretion and cooling phases may significantly change for different SN models. Therefore, a straightforward extraction of oscillation parameters from the bulk of the SN neutrino signal seems hopeless. Only features in the detected neutrino spectra that are independent of unknown SN parameters should be used in such an analysis.

In this talk we discuss the potential of the two most promising sources for such features: the modulations in the $\bar{\nu}_e$ spectra caused by the Earth matter [4, 5, 6] or by the passage of shock waves through the SN envelope [7, 8, 9]. Moreover, we show how the detection of the neutronization ν_e burst could help to break possible degeneracies in the case that θ_{13} is still unknown. In Tab. I it is shown the dependence of these three observables on three different neutrino mass schemes.

TABLE I: The presence of Earth-matter and shock wave effects in the $\bar{\nu}_e$ spectra and of the ν_e burst for different neutrino mixing scenarios.

Case	Hierarchy	$\sin^2\theta_{13}$	Earth	Shock	ν_e burst
A	Normal	$\gtrsim 10^{-3}$	Yes	No	No
B	Inverted	$\gtrsim 10^{-3}$	No	Yes	Yes
C	Any	$\lesssim 10^{-5}$	Yes	No	Yes

II. IDENTIFYING SIGNATURES OF THE SN SHOCK WAVE PROPAGATION

The neutrino spectra F_{ν_i} arriving at the Earth are determined by the primary neutrino spectra $F^0_{\nu_i}$ as well as the neutrino mixing scenario,

$$F_{\nu_i}(E,t) = \sum_j p_{ji}(E,t) F^0_{\nu_j}(E,t)\,, \qquad (1)$$

where p_{ji} is the conversion probability of a ν_j into ν_i after propagation through the SN mantle. The probabilities p_{ji} are basically determined by the number of resonances that the neutrinos traverse and their adiabaticity [21]. Both are directly connected to the neutrino mixing scheme. In contrast to the solar case, SN neutrinos must pass through two resonance layers: the H-resonance layer at $\rho_{\rm H} \sim 10^3$ g/cm^3 corresponding to $\Delta m^2_{\rm atm}$, and the L-resonance layer at $\rho_{\rm L} \sim 10$ g/cm^3 corresponding to $\Delta m^2_{\odot}$. Whereas the L-resonance is always adiabatic and in the neutrino channel, the adiabaticity of the H-resonance depends on the value of θ_{13}, and the resonance shows up in the neutrino or antineutrino channel for a normal or inverted mass hierarchy respectively [1].

During approximately the first two seconds after core bounce, the neutrino survival probabilities are constant in time and in energy for all three cases A,

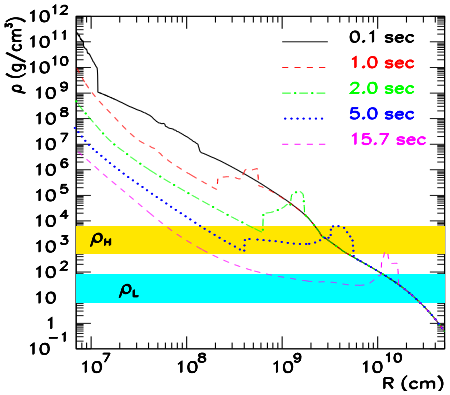

FIG. 1: Density profile at several instances after core bounce. The resonance layers $\rho_{\rm H}$ and $\rho_{\rm L}$ are also shown [9].

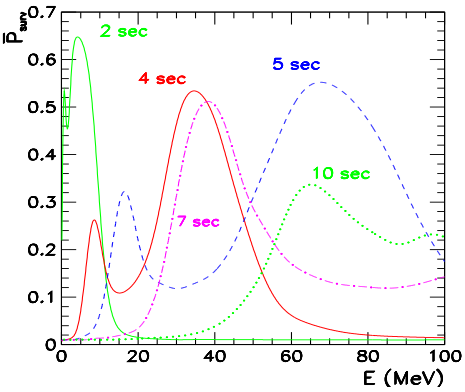

FIG. 2: Antineutrino survival probability $p_{\bar\nu_e\bar\nu_e}(E,t)$ as function of energy at different times averaging in energies with the energy-resolution of Super-Kamiokande. A density profile with a forward and reverse shock have been used, from Ref. [9].

B, and C. However, at $t \approx 2$ s the H-resonance layer is reached by the outgoing shock wave, see Fig. 1. The way the shock wave passage affects the neutrino propagation strongly depends on the neutrino mixing scenario: cases A and C will not show any evidence of shock wave propagation in the observed $\bar\nu_e$ spectrum, either because there is no resonance in the antineutrino channel as in scenario A, or because the resonance is always strongly non-adiabatic as in scenario C. However, in scenario B, the sudden change in density breaks the adiabaticity of the resonance, what leads to a time and energy dependence of the antineutrino survival probability $p_{\bar\nu_e\bar\nu_e}(E,t)$, see Fig.2. The presence of the shocks results in the appearance of bumps, one in the case of a unique forward shock or two if an additional reverse shock is present, in $p_{\bar\nu_e\bar\nu_e}(E,t)$ at those energies for which the resonance region is passed by the shock waves. All these structures move in time towards higher energies, as the shock waves reach regions with lower density, leading to observable consequences in the $\bar\nu_e$ spectrum.

A useful observable to detect effects of the shock propagation is the average of the measured positron energies, $\langle E_e\rangle$, produced in inverse beta decays $\bar\nu_e + p \to n + e^+$, the most important neutrino signal expected in a SN. In Figs. 3 and 4, we show $\langle E_e\rangle$ together with the one sigma errors expected for a megaton water Cherenkov detector and a SN in 10 kpc distance, with a time binning of 0.5 s. For the neutrino fluxes we use the parametrization suggested in Refs. [13, 14],

$$F^0_{\nu_j}(E) = \frac{\Phi_0(\nu_j)}{\langle E_0(\nu_j)\rangle}\frac{(\alpha_j+1)^{\alpha_j+1}}{\Gamma(\alpha_j+1)}\left(\frac{E}{\langle E_0(\nu_j)\rangle}\right)^{\alpha_j} \exp\left(-(\alpha_j+1)\frac{E}{\langle E_0(\nu_j)\rangle}\right) . \quad (2)$$

The values of the parameters used in the two models, $G1$ in Fig. 3 and $G2$ in Fig. 4, are given in Tab. II. The averaged energy is assumed to decrease linearly after 5 s.

TABLE II: The parameters of the used primary neutrino spectra models motivated from the SN simulations of the Garching (G1,G2) and the Livermore (L) group. The averaged energy is given in MeV and the pinching parameters $\alpha_{\bar\nu_e}$ and $\alpha_{\bar\nu_x}$ take the values 4 and 3, respectively.

Model	$\langle E_0(\bar\nu_e)\rangle$	$\langle E_0(\nu_x)\rangle$	$\Phi_0(\bar\nu_e)/\Phi_0(\nu_x)$
L	15	24	1.6
G1	15	18	0.8
G2	15	15	0.5

The effects of the shock wave propagation are clearly visible, and are independent of the assumptions about the initial neutrino spectra [9]. Moreover, it is not only possible to detect the shock wave propagation in general, but also to identify the specific imprints of the forward and reverse shock versus the forward shock only case. The signature of the reverse shock is its double-dip structure compared to the one-dip of a forward shock only. The observation of the details of the shock wave structure will be, though, tightly related to the absence of strong density fluctuations after the shock front [15, 16].

III. EARTH-MATTER EFFECTS

As it has been previously mentioned, before the shock wave reaches the H-resonance layer the dependence of the conversion probability in the cases A, B and C on the neutrino energy E is very weak. However, if neutrinos cross the Earth before reaching the detector, the conversion probabilities may become

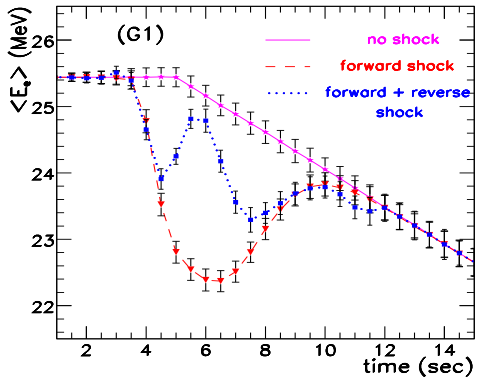

FIG. 3: The average energy of $\bar{\nu}p \to ne^+$ events binned in time for a static density profile, a profile with only a forward shock, and with forward and reverse shock. G1 model was assumed for the neutrino fluxes. The error bars represent 1 σ errors in any bin, from Ref. [9].

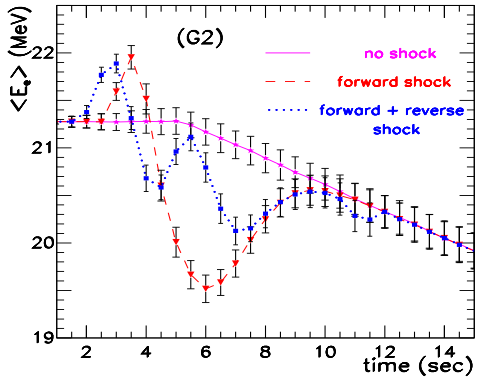

FIG. 4: Same as Fig. 3 for the G2 model. From Ref. [9].

energy-dependent and induce modulations in the neutrino energy spectrum. These modulations may be observed in the form of local peaks and valleys in the spectrum of the event rate $\sigma F^D_{\bar{\nu}_e}$ plotted as a function of $1/E$. These modulations arise in the antineutrino channel only in cases A and C. Therefore its observation would exclude case B. This distortion in the spectra could be measured by comparing the neutrino signal at two or more different detectors such that the neutrinos travel different distances through the Earth before reaching them [4, 17]. However these Earth matter effects can be also identified in a single detector [5, 6].

The net $\bar{\nu}_e$ flux at the detector may be written in the form

$$F^D_{\bar{\nu}_e} = \sin^2\theta_{12} F^0_{\bar{\nu}_x} + \cos^2\theta_{12} F^0_{\bar{\nu}_e} + \Delta F^0 \sum_{i=1}^{7} \bar{A}_i \sin^2(k_i y/2)\,, \qquad (3)$$

where y is the "inverse energy" parameter $y \equiv 12.5$ MeV$/E$, $\Delta F^0 \equiv (F^0_{\bar{\nu}_e} - F_{\bar{\nu}^0_x})$, and $\bar{A}_i$ depend only on the mixing parameters.

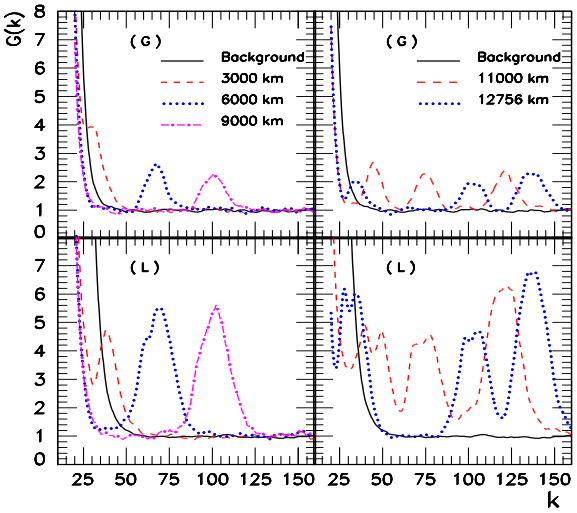

FIG. 5: Averaged power spectra in the case of a large scintillator detector for different SN models, G1 (top panels) and L (bottom panels), and distances travelled through the Earth, from Ref. [6].

The last term in Eq. (3) is the Earth oscillation term that contains up to seven analytically known frequencies k_i in y, the coefficients $\Delta F^0 \bar{A}_i$ being relatively slowly varying functions of y. The first two terms in Eq. (3) are also slowly varying functions of y, and hence contain frequencies in y that are much smaller than the k_i. The frequencies k_i are completely independent of the primary neutrino spectra, and can be determined to a good accuracy from the knowledge of the solar oscillation parameters, the Earth matter density, and the position of the SN in the sky [6]. The latter can be determined with sufficient precision even if the SN is optically obscured using the pointing capability of water Cherenkov neutrino detectors [18]. The power spectrum of N detected neutrino events is

$$G(k) \equiv \frac{1}{N}\left|\sum_{i=1}^{N} e^{iky_i}\right|^2 . \qquad (4)$$

In the absence of Earth effect modulations, $G(k)$ has an average value of one for $k \gtrsim 40$. The region $k \lesssim 40$ is dominated by the "0-peak", which is a manifestation of the low frequency terms in Eq. (3). Identifying Earth effects is equivalent to observing excess power in $G(k)$ around the known frequencies k_i. In Fig. 5 we show the averaged power spectra in the case of a 32 kton scintillator detector for neutrinos travelling only through the Earth mantle (left panels) and traversing both mantle and core (right panels). It is

possible to observe how in the former case only one peak is present, whereas in the case that neutrinos go through the core more frequencies arise. The model independence of the peak positions may be confirmed by comparing the top and bottom panels.

Since in the real world the presence of fluctuations in the signal, see Fig. 6, will spoil any naive theoretical peak, we need to introduce a prescription to carry out the analysis. One possibility is to consider the area around the expected position of the peak. The area under the power spectrum between two fixed frequencies $k_{\rm min}$ and $k_{\rm max}$ is on an average $(k_{\rm max} - k_{\rm min})$. In the absence of Earth effects, this area will have a distribution centered around this mean. The Earth effect peaks tend to increase this area. The confidence level of peak identification, p_α, may then be defined as the fraction of the area of the background distribution that is less than the actual area measured.

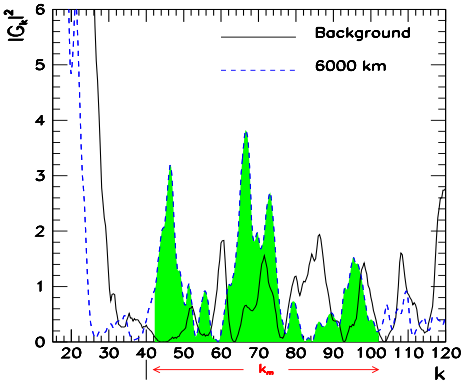

FIG. 6: Realistic power spectrum from a single simulation, from Ref. [6] .

In Fig. 7, we compare p_{95} obtained with a 32 kton scintillator detector and a megaton water Cherenkov detector assuming a SN at 10 kpc and the $G1$ model for neutrino fluxes. In the latter case, as neutrinos travel more and more distance in the mantle the peak moves to higher k values, and due to the high k suppression, the efficiency of peak identification decreases. When the neutrinos start traversing the core, additional low k peaks are generated and the efficiency increases again. The identification of Earth matter effects excludes case B, and is thus complementary to the observation of shock wave effects.

IV. NEUTRONIZATION $\nu_{\rm e}$ BURST

If the value of θ_{13} is unknown, a degeneracy exists between case A and C. Both scenarios predict the same $\bar{\nu}_e$ signature in a water Cherenkov detector, and therefore the previous two observables are not useful to disentangle them. In this case, the additional in-

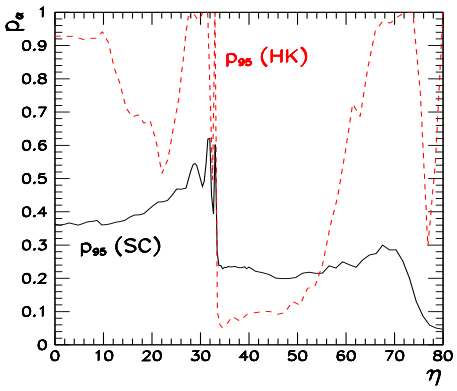

FIG. 7: Comparison of p_{95} as a function of nadir angle η for a 32 kton scintillator (SC) and a megaton water Cherenkov (HK) detector [6].

formation encoded in the ν_e neutrinos emitted during the neutronization burst can fix the range of θ_{13} as well as the neutrino mass hierarchy.

The prompt neutronization burst takes place during the first ~ 25 ms after the core bounce with a typical full width half maximum of 5–7 ms and a peak luminosity of 3.3–$3.5\times10^{53}\,{\rm erg\,s^{-1}}$. The striking similarity of the neutrino emission characteristics despite the variability in the properties of the pre-collapse cores is caused by a regulation mechanism between electron number fraction and target abundances for electron capture which establishes similar electron fractions in the inner core during collapse. This leads to a convergence of the structure of the central part of the collapsing cores and only small differences in the evolution of different progenitors until shock breakout. The small dependence of the neutronization burst on, e.g., the progenitor mass can be verified in Fig. 8 (cf. also Refs. [19, 20]).

Taking into account that the SN will be likely obscured by dust and a good estimation of the distance will not be possible, the time structure of the detected neutrino signal should be used as signature for the neutronization burst [19]. Since the event number in current and proposed charged-current ν_e detectors is not high enough to allow for a detailed time analysis, we discuss only the case of a megaton water Cherenkov detector. Here one has to consider the ν_e elastic scattering on electrons, which is affected by several backgrounds like inverse beta decay or reactions on oxygen. This background can be substantially reduced by using angular and energy cuts, as well as Gadolinium to tag neutrons from inverse beta decays. The sample of elastic scattering events still contains the irreducible background of scattering on electrons of other neutrino flavors than ν_e, but this contamination does not affect the possibility to disentangle the different neutrino scenarios [19].

The time evolution of the signal depends strongly on the neutrino mixing scheme. In case A, the ν_e survival probability is close to zero, and therefore the peak structure observed in the initial ν_e luminosity is absent. On the contrary, in case C, 30% of the original ν_e remain as ν_e whereas 70% are converted into ν_x. Since the cross section of ν_e on electrons is much larger than that of ν_x, the signal is dominated by the contribution of ν_e. These ν_e's follow the time evolution of L_{ν_e}, and thus lead to a clear peak in the signal.

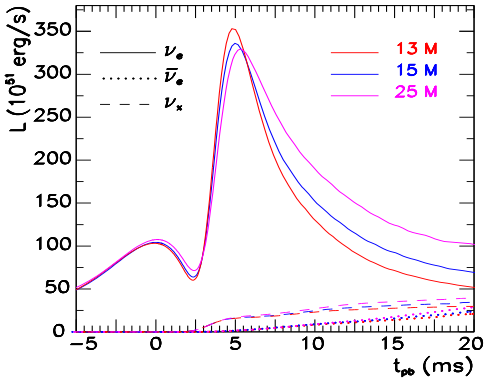

FIG. 8: Neutrino luminosities as function of time for different progenitor masses, from Ref. [19].

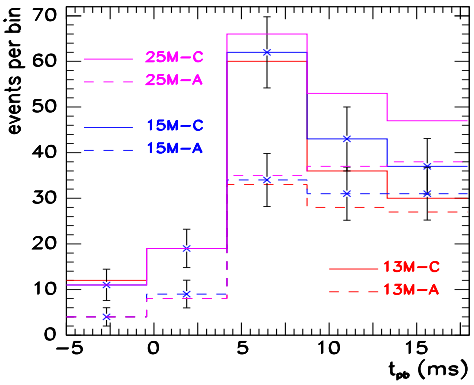

FIG. 9: Number of $\nu e \to \nu e$ events per time bin in a megaton water Cherenkov detector for a SN at 10 kpc for cases A (dashed lines) and C (solid lines) and for different progenitor masses. Statistical errors are also shown for the 15 $M_\odot$ case [19].

In Fig. 9 we show the expected neutrino signal from $t = -5$ to 18 ms for different progenitor masses, and for the mixing scenarios A and C. The peak structure can be clearly seen in case C, but not in case A [19]. Including recent improvements of the electron capture rates or uncertainties in the nuclear equation of state has only little effect on the neutronization peak compared to the size of the statistical fluctuations. Therefore the observation of a peak in the first milliseconds of the neutrino signal would rule out case A.

V. SUMMARY

A reliable determination of neutrino parameters using SN neutrinos should be independent from the primary neutrino fluxes produced during the accretion and cooling phase of the SN. Earth-matter effects and the passage of SN shocks through the H-resonance both introduce unique modulations in the neutrino energy spectrum that allow one their identification without knowledge of the primary neutrino spectra. While the observation of Earth-matter effects in the $\bar{\nu}_e$ energy spectrum rules out case B, modulations in the $\bar{\nu}_e$ time spectrum identify case B. If the value of θ_{13} would be known to be large, then the neutrino mass hierarchy would be identified. Otherwise, the detection of the neutronization ν_e peak—a robust feature of all modern SN simulations—can break the remaining degeneracy between A and C.

Acknowledgments

I am greatly grateful to the local organizers for the warm hospitality during the Conference. I would also like to thank M. Frigerio, G. Senjanovic, and S. Thomas for very pleasant and interesting discussions. The results presented in this talk were derived in collaboration with M. Kachelrieß, A. S. Dighe, G. G. Raffelt, H. -Th. Janka, L. Scheck, R. Buras, A. Marek, and M. Rampp. This work has been supported by the Juan de la Cierva programme, an ERG from the European Comission, and by the Spanish grant FPA2005-01269.

[1] A. S. Dighe and A. Y. Smirnov, "Identifying the neutrino mass spectrum from the neutrino burst from a supernova," Phys. Rev. D **62**, 033007 (2000) [arXiv:hep-ph/9907423].

[2] C. Lunardini and A. Y. Smirnov, "Probing the neutrino mass hierarchy and the 13-mixing with supernovae," JCAP **0306**, 009 (2003) [arXiv:hep-ph/0302033].

[3] K. Takahashi and K. Sato, "Effects of neutrino oscillation on supernova neutrino: Inverted mass hierarchy," Nucl. Phys. A **718**, 455 (2003).
[4] C. Lunardini and A. Y. Smirnov, "Supernova neutrinos: Earth matter effects and neutrino mass spectrum," Nucl. Phys. B **616**, 307 (2001) [arXiv:hep-ph/0106149].
[5] A. S. Dighe, M. T. Keil and G. G. Raffelt, "Identifying earth matter effects on supernova neutrinos at a single detector," JCAP **0306**, 006 (2003) [arXiv:hep-ph/0304150].
[6] A. S. Dighe, M. Kachelrieß, G. G. Raffelt and R. Tomàs, "Signatures of supernova neutrino oscillations in the earth mantle and core," JCAP **0401**, 004 (2004) [arXiv:hep-ph/0311172].
[7] R. C. Schirato and G. M. Fuller, "Connection between supernova shocks, flavor transformation, and the neutrino signal," arXiv:astro-ph/0205390.
[8] G. L. Fogli, E. Lisi, D. Montanino and A. Mirizzi, "Analysis of energy- and time-dependence of supernova shock effects on neutrino crossing probabilities," Phys. Rev. D **68**, 033005 (2003) [arXiv:hep-ph/0304056].
[9] R. Tomàs, M. Kachelrieß, G. Raffelt, A. Dighe, H. T. Janka and L. Scheck, "Neutrino signatures of supernova shock and reverse shock propagation," JCAP **0409**, 015 (2004) [arXiv:astro-ph/0407132].
[10] H. Duan, G. M. Fuller, J. Carlson and Y. Z. Qian, "Simulation of coherent non-linear neutrino flavor transformation in the supernova environment. I: Correlated neutrino trajectories," Phys. Rev. D **74**, 105014 (2006) [arXiv:astro-ph/0606616].
[11] H. Duan, G. M. Fuller, J. Carlson and Y. Z. Qian, "Coherent development of neutrino flavor in the supernova environment," Phys. Rev. Lett. **97**, 241101 (2006) [arXiv:astro-ph/0608050].
[12] S. Hannestad, G. G. Raffelt, G. Sigl and Y. Y. Y. Wong, "Self-induced conversion in dense neutrino gases: Pendulum in flavour space," Phys. Rev. D **74**, 105010 (2006) [arXiv:astro-ph/0608695].
[13] M. T. Keil, G. G. Raffelt and H. T. Janka, "Monte Carlo study of supernova neutrino spectra formation," Astrophys. J. **590**, 971 (2003) [arXiv:astro-ph/0208035].
[14] M. T. Keil, "Supernova neutrino spectra and applications to flavor oscillations," arXiv:astro-ph/0308228.
[15] G. L. Fogli, E. Lisi, A. Mirizzi and D. Montanino, "Damping of supernova neutrino transitions in stochastic shock-wave density profiles," JCAP **0606**, 012 (2006) [arXiv:hep-ph/0603033].
[16] A. Friedland and A. Gruzinov, "Neutrino signatures of supernova turbulence," arXiv:astro-ph/0607244.
[17] A. S. Dighe, M. T. Keil and G. G. Raffelt, "Detecting the neutrino mass hierarchy with a supernova at IceCube," JCAP **0306**, 005 (2003) [arXiv:hep-ph/0303210].
[18] R. Tomàs, D. Semikoz, G. G. Raffelt, M. Kachelrieß and A. S. Dighe, Phys. Rev. D **68**, 093013 (2003) [arXiv:hep-ph/0307050].
[19] M. Kachelrieß, R. Tomàs, R. Buras, H. T. Janka, A. Marek and M. Rampp, "Exploiting the neutronization burst of a galactic supernova," Phys. Rev. D **71**, 063003 (2005) [arXiv:astro-ph/0412082].
[20] K. Takahashi, K. Sato, A. Burrows and T. A. Thompson, "Supernova neutrinos, neutrino oscillations, and the mass of the progenitor star," Phys. Rev. D **68**, 113009 (2003) [arXiv:hep-ph/0306056].
[21] In this talk we shall not consider the possible presence of collective flavor neutrino conversions driven by neutrino-neutrino interactions [10, 11, 12].